PHYSICAL REVIEW B **81**, 245124 (2010)

Calculations of electron energy loss and x-ray absorption spectra in periodic systems without a supercell

K. Jorissen and J. J. Rehr*
Department of Physics, University of Washington, Seattle, Washington 98195, USA
(Received 8 February 2010; revised manuscript received 6 June 2010; published 23 June 2010)

Ab initio calculations of relativistic core-level electron-energy-loss spectra and x-ray absorption spectra in periodic systems are carried out using an impurity Green's function formalism without the need for a supercell. The approach is based on a hybrid scheme incorporating a reciprocal space calculation of the multiple-scattering equations, together with a real-space calculation of the excitation spectrum with a statically screened core-hole potential. The approach accounts for core-hole effects in deep-core spectroscopies of periodic systems while circumventing the supercell convergence issues encountered with conventional band-structure codes. The approach is implemented in an extension of the real-space Green's function code FEFF. Illustrative calculations are presented for the *K* edges of C (diamond) and Cu, and the N *K* edge of GaN.

DOI: 10.1103/PhysRevB.81.245124 PACS number(s): 79.20.Uv, 71.15.Qe

I. INTRODUCTION

Electron-energy-loss spectroscopy (EELS) and x-ray absorption spectra (XAS) are important core-level spectroscopy techniques for understanding the structural, chemical, and electronic information about a particular material. EELS measures the energy loss of a beam of high-energy (typically of order 100 keV) electrons, propagated through a sample in electron microscopes,[1] while XAS measures the attenuation of an x-ray beam. Apart from relativistic effects[2] these core-level spectra are essentially the identical. The spectra encompass both extended fine structure and near-edge structure. For electron energy loss, these include extended energy loss fine structure (EXELFS) and energy loss near edge structure (ELNES). For x-ray absorption, they include extended x-ray absorption fine structure (EXAFS) and x-ray absorption near edge structure (XANES). As there is no quantitative experimental approach for analyzing near-edge spectra, *ab initio* calculations are often used to interpret the experimental data. One commonly used method is based on the real-space Green's function (RSGF) code FEFF.[1–6] The real-space formalism in FEFF treats the *extended* energy loss region very efficiently and permits calculations of the spectra in complex systems over hundreds of electron volt in terms of a finite multiple-scattering expansion. In contrast, calculations of the *near-edge* spectra must usually be carried to all orders of multiple-scattering using a matrix inversion algorithm, which is a real-space analog of the Korringa-Kohn-Rostoker (KKR) band-structure approach that includes the core-hole potential. We focus here on the calculation of ELNES, corresponding to inelastic losses from the excitation of an electron from a deep-core level, i.e., for core levels below about −50 eV, into unoccupied states up to about 50 eV above the threshold (or Fermi energy) in the system. Similar considerations also apply to XAS and other deep-core-excitation spectra such as nonresonant inelastic x-ray scattering (NRIXS). Because EELS is an absorption technique and the initial deep-core-level states are sharply defined in energy, such core-loss signals predominantly reflect the electronic structure of excited, unoccupied electron states. In particular, apart from a smooth background cross-section factor and broadening, the shape of an ionization edge roughly corresponds to the unoccupied angular momentum projected density of electron states, where the allowed states are fixed, e.g., by dipole selection rules.

Within an effective independent particle approximation, the excited "photoelectron states" must be calculated in the presence of an appropriately screened core hole. In addition, inelastic losses and core-hole lifetime give the photoelectron a finite range, typically of order 5–20 Å for ELNES energies. The nature of the screening is still a matter of debate, as various approximations for the core-hole potential are commonly used. These include for example, a fully screened potential based on the final-state rule (FSR), i.e., the final-state Hamiltonian in the presence of the core hole; the $Z+1$ approximation; transition-state models; and linear random-phase-approximation (RPA) screening as in the Bethe-Salpeter equation (BSE).[7,8] In contrast to the case of valence excitations,[9,10] the screened core hole is well localized and the range of the photoelectron is short in deep-core spectroscopies, and hence long-range core-hole effects are not important. Nevertheless, the symmetry of the final-state one-electron Hamiltonian is broken because of the core hole, even for perfect crystals. Thus, the calculation of excitation properties can be cast essentially as a localized, isolated impurity problem in an otherwise periodic system, with the net signal averaged over all absorption sites. Consequently, we must revisit the age-old dilemma of choosing between real-space and reciprocal-space approaches for such calculations. The choice depends on whether short- or long-range effects dominate.

For calculations of EELS of *aperiodic* materials (e.g., amorphous materials, alloys, and defect systems), a cluster method such as the RSGF approach is often the method of choice. This method has been implemented for relativistic EELS calculations in the FEFF codes[2] and is widely used for simulating the spectra in such complex materials. Incorporating the core hole in the RSGF using the FSR (i.e., a fully screened self-consistently determined core hole) or other screened core-hole approximations is straightforward, provided that the cluster is large enough compared to the inelastic mean-free path, which is of order 10 Å. For *periodic*

materials, on the other hand, RSGF calculations can be less appropriate for treating the ground states of a perfect crystal in which the excitation takes place. The reason is that the infinite crystal must be approximated by a finite cluster of ordered atoms, the size of which an unphysical parameter that must be converged to avoid finite-size artifacts.

Intuitively, a reciprocal-space formalism might seem to be a better choice for calculating the EELS for a periodic crystal. However, as mentioned above, in the presence of a core hole, the excitation problem is effectively mapped onto an impurity problem which breaks the symmetry of the crystal. This can still be treated approximately by imposing periodic boundary conditions (PBC). However, PBC places images of the "original" core hole into every unit cell so that it becomes necessary to use an artificially enlarged *supercell* to suppress unphysical hole-hole interactions and related artifacts in the spectrum. Thus the supercell size is again an unphysical parameter that must be converged. The resources required for such PBC-FSR calculations rise dramatically, typically as the cube of the dimension of the supercell in typical calculations of electronic structure and spectra. A number of codes based on the supercell approach currently exist.[11–13]

The above considerations suggest that efficient calculations of EELS and XAS of crystals may need to blend both views—real and reciprocal. Therefore we now propose a hybrid approach for the calculation of deep-core excitation spectra of periodic systems in two steps: (i) calculate the ground state of the perfect crystal in reciprocal space and (ii) calculate the excitation spectra in real space with the addition of an appropriately screened core hole. In (i) a conventional unit cell is used while in (ii) the calculation is carried out in real space without any particular unit cell. In this way, supercells are completely avoided. This hybrid approach is similar to that introduced by Beeby[14,15] for impurity KKR calculations[16,17] of the electronic properties of impurities with real-valued Hamiltonians. However, our application to core-hole EELS and XAS spectroscopy has a number of novel features. Also the approach has the potential to improve theoretical calculations of EELS and XAS in many cases. With respect to band-structure codes, the description of the excitation is improved, and with respect to real-space codes such as FEFF, the description of ground state properties of periodic solids is improved. Our approach also makes possible a straightforward comparison between our hybrid approach and conventional supercell band-structure approaches. This impurity Green's function approach is now implemented in an extension of the FEFF9 code.

The theory relevant to the reciprocal space extension of FEFF is described in Sec. II while Secs. III and IV briefly describe computational considerations and convergence issues. Finally, some illustrative applications are given in Secs. V and VI. In particular, we discuss supercell size convergence and the equivalence of short-range and long-range results. We stress that, while this paper focuses on EELS, the approach discussed here also applies to XAS, NRIXS, and related deep-core spectroscopies, for which the underlying physics is quite similar.

II. *K*-SPACE MULTIPLE SCATTERING FORMALISM

In the RSGF theory, the EELS or XAS spectrum is obtained from local matrix elements of the Green's function

$$\mu(\omega) \sim \mathrm{Im}\sum_i \langle i|d^* G(E) d|i\rangle \theta(E - E_f), \tag{1}$$

which is formally equivalent to Fermi's golden rule. Here, i is the initial core state of the system, $E=E_i+\omega$ is the final-state photoelectron energy, and d is the dipole operator for EELS or XAS excitations. The expression for the nonrelativistic EELS spectrum at small momentum transfer is similar but with d replaced by $e^{i\boldsymbol{qr}}$, where $\boldsymbol{q}$ is the momentum transfer. For relativistic beam energies, the transition operator d contains additional relativistic corrections[2] but the precise form is not essential here. The Green's function G of the electron in the crystal is calculated from the free electron propagator G^0 and the scattering matrices $\boldsymbol{t_n}$ of sites $\boldsymbol{n}$ in the crystal. For excited states the free-electron propagator $G^0 = [E-h-\Sigma(E)]^{-1}$ is the damped quasiparticle Green's function as calculated in FEFF with a complex GW self-energy $\Sigma(E)$ that replaces the exchange-correlation potential in ground-state density-functional calculations, and h is the Hartree potential of the final-state photoelectron, which is calculated self-consistently in the presence of a screened core hole.[5] The full Green's function G is calculated by summing over all possible multiple scattering paths of the photoelectron of energy E [first equality in Eq. (2) below]. For EXELFS or EXAFS, that is for energy losses of more than about 50 eV beyond the edge threshold, when inelastic losses are strong, this explicit multiple-scattering path expansion converges well with increasing scattering path length. In order to calculate the absorption spectrum near-edge structure, i.e., ELNES or XANES within 50 eV of threshold, the full multiple scattering (FMS) approach in real space has been developed. For FMS, one limits the number of atoms to a small cluster around the absorber (typically 100–300 atoms, depending on the inelastic mean-free path) but sums implicitly over all scattering paths within this cluster using a matrix inversion equivalent to the KKR multiple-scattering equations[4]

$$\begin{aligned} G &= G^0 + G^0 t G^0 + G^0 t G^0 t G^0 + \cdots \\ &= G^0[1 - tG^0]^{-1} = [1 - G^0 t]^{-1} G^0. \end{aligned} \tag{2}$$

For calculation purposes, the quantities in Eq. (2) are represented as matrices in a site and angular momentum basis $|\mathbf{n},\mathbf{L}\rangle$, where $\mathbf{n}$ denotes a site index and $\mathbf{L}=l,m$ the angular momentum indices. When calculating Eq. (2) in real space for a crystal, one needs to truncate the matrices at some maximum radius in real space. Sometimes the convergence of the spectrum with respect to this finite cluster size can be computationally demanding. For example, the diamond K edge of C (diamond) requires at least 600 atoms in a FMS calculation due to the long mean-free path in the near-edge region. In contrast, the periodicity of crystals makes it more efficient and elegant to carry out the calculation in $\boldsymbol{k}$ space. This way, it is possible to treat the full crystal without introducing a cut-off radius. This was first described in detail by Beeby[14] and we proceed analogously.

The $\boldsymbol{k}$-space KKR structure constants $\boldsymbol{K}$ are defined as the lattice Fourier transforms of the real-space free propagator matrix elements G^0

$$K_{\alpha\beta}(\boldsymbol{k}) = \lim_{N\to\infty} N^{-1} \sum_{\substack{i\neq j \\ \text{lattice vectors}}}^{N} e^{i\boldsymbol{k}\cdot\boldsymbol{r}_{ij}} G^0_{i\alpha,j\beta};$$

$$G^0_{i\alpha,j\beta} = G^0[(\boldsymbol{r}_i + \boldsymbol{a}_\alpha) - (\boldsymbol{r}_j + \boldsymbol{a}_\beta)]. \tag{3}$$

They are discussed in more detail in the appendix. Notationally, we index atoms in real space by $\boldsymbol{n},\boldsymbol{n}',\ldots$ while the same atoms are specified in reciprocal space using a lattice vector $i,j,\ldots$ and an index $\alpha,\beta,\ldots$ specifying their positions within the unit cell. Thus $G_{\boldsymbol{n},\boldsymbol{n}'} \equiv G_{i\alpha,j\beta}$. The inverse transformation is

$$\Omega_{\mathrm{BZ}}^{-1} \int_{\mathrm{BZ}} d\boldsymbol{k} K_{\alpha\beta}(\boldsymbol{k}) e^{-i\boldsymbol{k}\cdot\boldsymbol{r}_{ij}} = G^0_{i\alpha,j\beta}. \tag{4}$$

We now calculate the electronic structure of the ground-state crystal, that is, with no core hole present yet. Introducing the $\boldsymbol{k}$-space KKR structure constants in Eq. (2) leads to

$$G_{nn'} = \int_{\mathrm{BZ}} d\boldsymbol{k} e^{-i\boldsymbol{k}\cdot\boldsymbol{r}_{ii'}} [(1-KT)^{-1}K]_{\alpha\alpha'}; \quad T_{\alpha\alpha'} = t_\alpha \delta_{\alpha\alpha'}, \tag{5}$$

where K and T are matrices in a site and angular momentum basis, $t_\alpha = \exp(i\delta_l)\sin\delta_l$ with the sites now corresponding to the atoms of the unit cell of the crystal (a finite number). Equation (5) yields the real-space Green's function, from which one can obtain the electronic structure and excitation spectra without any finite cluster approximations. Also, the poles of the integrand of Eq. (5) yield the band structure. This is formally equivalent to KKR theory,[16,17] where the band structure is obtained from the pole singularities of the scattering path operator $\boldsymbol{\tau}(\boldsymbol{k})$

$$\tau(\boldsymbol{k}) = [K(\boldsymbol{k}) - t^{-1}]^{-1}. \tag{6}$$

If the unit cell contains only one atom, the indices α can be dropped in Eqs. (3) and (5), thereby simplifying the equations to

$$K(\boldsymbol{k}) = \lim_{N\to\infty} \sum_{\substack{j\neq 1 \\ \text{lattice vectors}}}^{N} e^{i\boldsymbol{k}\cdot\boldsymbol{r}_{1j}} G^0_{1,j}, \tag{7}$$

$$G_{nn'} = \int_{\mathrm{BZ}} d\boldsymbol{k} e^{-i\boldsymbol{k}\cdot\boldsymbol{r}_{ii'}} [1 - K(\boldsymbol{k})t]^{-1} K(\boldsymbol{k}). \tag{8}$$

These are equivalent to the results of Schaich[18] and Beeby[15] for monatomic crystals.

It is now straightforward to add a well-localized core hole to the above formalism, assuming that only the potential at a single site is changed. This is done entirely in real space, avoiding the problems with PBC and supercells discussed in the introduction. The impurity KKR approach treats impurities in precisely the same way.[14] First, we start with the solution G^p for the perfect (ground-state) crystal with scattering matrix T^p, calculated using Eq. (5). The imperfect crystal with a core hole has the same KKR structure constants as the perfect system but with a scattering matrix T^i that differs from T^p only in one site block corresponding to the core-hole atom. Its Green's function G^i is now given by simple matrix algebra

$$G^i = (1 - G^0T^p - G^0T)^{-1}G^0 = (1 - G^pT)^{-1}G^p, \quad T \equiv T^i - T^p. \tag{9}$$

When T is nonzero in one block only, the Green's function between sites $\boldsymbol{n}$ and $\boldsymbol{n}'$ is given by

$$G_{nn'} = (1-\delta_{nc})G^p_{nn'} + [\delta_{nc}1 + (1-\delta_{nc})G^p_{nc}t^i_c] \times (1 - G^p_{cc}t^i_c)^{-1}G^p_{cn'}, \tag{10}$$

where c is the index of the core hole. In particular, we need for the EELS spectrum

$$G_{cc} = (1 - G^p_{cc}t^i_c)^{-1}G^p_{cc}. \tag{11}$$

III. METHODS OF CALCULATION

The above approach for calculating EELS has been implemented in the FEFF9 code. With the addition of the reciprocal space approach, the code now offers three formally equivalent ways of calculating the Green's function

$$G = G_0 + G_0tG_0 + G_0tG_0tG_0 + \cdots, \tag{12}$$

$$G = G_0[1 - tG_0]^{-1}, \tag{13}$$

$$G = \int_{\mathrm{BZ}} d\boldsymbol{k} G_0(\boldsymbol{k})[1 - tG_0(\boldsymbol{k})]^{-1}. \tag{14}$$

The XAS and EELS are then calculated using Eq. (1) with G from one of Eqs. (12)–(14). The local density of states (DOS) can also be obtained from the imaginary part of $G(E)$, i.e., the lDOS is $\rho_l(E) = -(1/\pi)\mathrm{Im}\, G_l(E)$. Equation (12) is the multiple-scattering path expansion (MSPE) and is appropriate for calculating EXELFS and EXAFS many hundreds of electron volts above threshold. Equation (13), the FMS in real space,[4] is appropriate for ELNES and XANES of aperiodic systems. Equation (14), the $\boldsymbol{k}$-space approach of Sec. II, is appropriate for ELNES and XANES of crystals. In all three cases, the core hole is treated in real space. In the PE and FMS approaches, it amounts to changing the t matrix on only one atom (the absorbing atom) in the real-space cluster of the calculation. In the $\boldsymbol{k}$-space approach, the impurity perturbation is added in real space after evaluating Eq. (14)

$$G_{ch} = G[1 - \Delta t_{ch}G]^{-1}. \tag{15}$$

Considering computational efficiency, we note that all quantities in Eqs. (12)–(15) are matrices in a site and angular momentum basis $|\mathbf{n},\mathbf{L}\rangle$. Similar angular momentum cutoffs are needed in all cases. The computational cost of the calculation is dominated by the matrix inversions in Eq. (13) and (14). Real-space FMS requires one inversion of a large matrix of dimension given by the number of atoms in the cluster

times the size of the angular momentum basis $(l_{max}+1)^2$ for real space FMS, where l_{max} is the maximum angular momentum. The $\boldsymbol{k}$-space calculations involve inversion of a small matrix of dimension given by the number of atoms in the unit cell for each k vector used to sample the Brillouin zone (BZ) integral. As the unit cell of a crystal becomes larger, fewer k points are typically needed but the calculations become slower with increasing unit cell size. Since one typically needs a cluster of 300 atoms for real-space calculations, the reciprocal space treatment is especially advantageous for crystals with small unit cells containing only a few atoms. For EXELFS, at energy losses more than 50–70 eV above threshold, the angular momentum cutoffs required for converged results gradually increase. At the same time, the MSPE formalism becomes increasingly more accurate in representing the spectrum. It is therefore advantageous to use the real-space MSPE calculations for the extended fine structure even for crystals. Thus reciprocal space calculations are now straightforward to use with FEFF9.[19]

Typically, the element of which one calculates a particular edge occurs many times in the crystal. As the electron beam causes many excitations during the experiment, the contributions of all occurrences of the element must be summed. It is appropriate to do the sum incoherently. The excitations can be treated as independent since core loss EELS excitations are localized due to the spatial confinement of the initial core state of the sample and are sufficiently rare that they are unlikely to influence each other. Thus, it is sufficient to calculate the spectra of each atom independently and simply take the average. In the case of crystals, one sums the spectra of each atom in the unit cell. For example, graphite [highly oriented pyrolytic graphite (HOPG)] contains four carbon atoms, two of which are crystallographically inequivalent (i.e., have a different environment and therefore different local electronic structure). The other two differ from the first two only by a symmetry element of the crystal point group. Now if one wants to calculate an orientation-averaged C K spectrum (to simulate a polycrystalline sample), it is sufficient to calculate the spectrum for the two inequivalent positions, multiply each spectrum by the number of atoms it represents (two, in this case), and add them. If one wants to calculate an orientation-resolved spectrum, it is necessary to add four individual spectra, as even the crystallographically equivalent atoms are oriented differently with respect to the beam and contribute differently. Each inequivalent site generally requires a new core-hole calculation whereas equivalent sites can be obtained by appropriately rotating the local electronic structure (or, equivalently, the electron beam). Such summations are not currently automated in FEFF9 but are easily done by hand. Note that, although FEFF9 also has an option to calculate configurational averages for the fine structure, we recommend using the technique described here instead, as it will generally be much more accurate for the near edge.

IV. CONVERGENCE OF K-SPACE CALCULATIONS

In $\boldsymbol{k}$-space calculations of the propagator $G(E)$ in Eq. (14), the Green's function is obtained by numerically evaluating an integral over a Brillouin zone. FEFF9 uses the conventional tetrahedron integration approach of Blöchl *et al.*[20] The number of k vectors in the integration grid is a key convergence parameter in the calculation. It is difficult to give a general prescription for the number of k points to use since the required number for convergence depends on the size of the Brillouin zone (which is inversely proportional to the size of the real-space unit cell), the complexity of the band structure and the desired accuracy. In any case, it is not necessary to converge fine details of the electronic structure when simulating a spectrum with large lifetime broadening. However, we find that in FEFF k meshes on the order of 10^3 points are typically sufficient to obtain converged results for crystals with small unit cells.

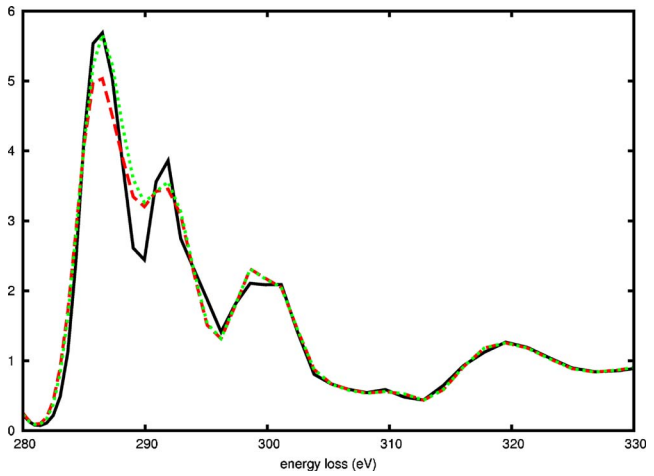

FIG. 1. (Color online) Convergence of the C K-edge ELNES of diamond, calculated using FEFF9 with the impurity Green's function approach, with varying numbers of k points used for Brillouin-zone integration: 100 (black, solid line), 1000 (red, long dashes), and 5000 (green, short dashes). Above 5000 k points, the spectrum is fully converged.

We illustrate in Fig. 1 the impurity Green's function approach for the C K-edge ELNES of diamond as calculated with FEFF9 using Eq. (14) in Eq. (1). Fair convergence is achieved for 1000 k points and excellent convergence for 5000 k points. No substantial change is observed when increasing to 25 000 k points.

As a second example, the total ground-state DOS of HOPG graphite in the absence of a core hole $\rho(E)=\Sigma_l \rho_l(E)$ is shown in Fig. 2. Since the ground state DOS lacks final-state broadening, it is much sharper than the ELNES and convergence is slower with 5000 k points needed for a converged result. In particular, the zero width band gap at the Fermi level ($E_F=-13.8$ eV in Fig. 2) takes 3000 k points to converge well.

V. CORE-LEVEL EELS WITHOUT A SUPERCELL

Calculations of core-level spectra are typically carried out with a self-consistently screened static core hole, as in the FSR. Such FSR calculations often yield results that are significantly better than ground-state calculations. More sophisticated calculations require the BSE.[8] For deep-core spectra,

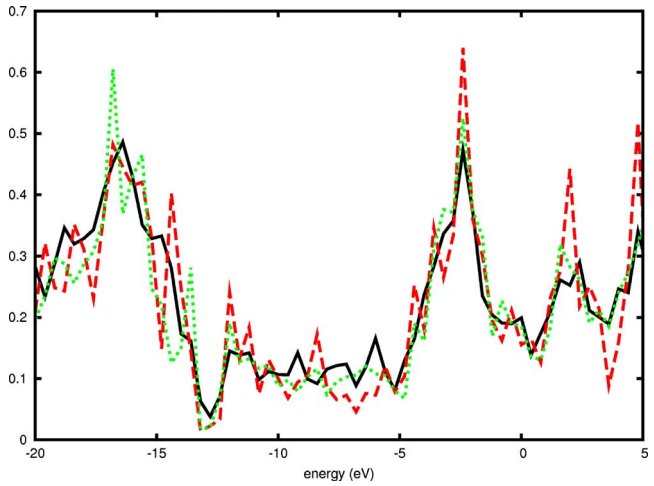

FIG. 2. (Color online) Total density of states of graphite $\rho(E)$, calculated using the $\boldsymbol{k}$-space approach as implemented in FEFF9, and its convergence with the number of k points used for BZ integration. We show calculations using 1000 (black, solid line), 3000 (red, long dashes), and 5000 (green, short dashes) k points in the full Brillouin zone. The Fermi-level $\boldsymbol{E_F}$ is at −13.8 eV relative to the vacuum level.

the use of a static RPA screened core hole provides a good approximation to the BSE.[17] However, while the FSR breaks the symmetry of a crystal, calculations of XAS and ELNES are often done using band-structure codes with PBC. This necessitates the use of a supercell, leading to convergence issues with respect to the size of the supercell. The use of PBC replicates core hole atoms throughout the crystal at the rate of one impurity per supercell so supercell size convergence requires that these be far enough apart to mimic a crystal in which there is only one excitation. All interactions between neighboring core-hole atoms are unphysical and must be suppressed by making the supercell larger. In principle, this requires a convergence study for each material under consideration. There are many successful examples of convergence studies in literature.[11,21,22] However, in some cases convergence is difficult or impractical to reach with current computational tools. A notorious case is the C K edge of diamond.[13] Moreover, supercell convergence studies can require significant effort and computer time.

Below we illustrate our "core hole without the supercell" approach for the N K edge of wurtzite (or hexagonal) GaN. Here references to reciprocal-space FEFF9 calculations always mean the ground state Green's function is calculated in reciprocal space, and the core hole added in real space, as outlined in Sec. II. Measurements were taken from Moreno *et al.*[23] In Fig. 3(a) we compare experimental data measured in the [100] orientation to different FEFF9 calculations. Real-space calculations are already quite successful for simulations of this particular edge but it is clear that our treatment using the reciprocal-space ground state and a real-space core hole yields even better agreement with experiment, improving, in particular, the description of the feature at 405-eV loss and the amplitude of the edge onset at 401-eV loss. We also note that the full reciprocal space calculation gives better results than a hybrid calculation in which the potentials and

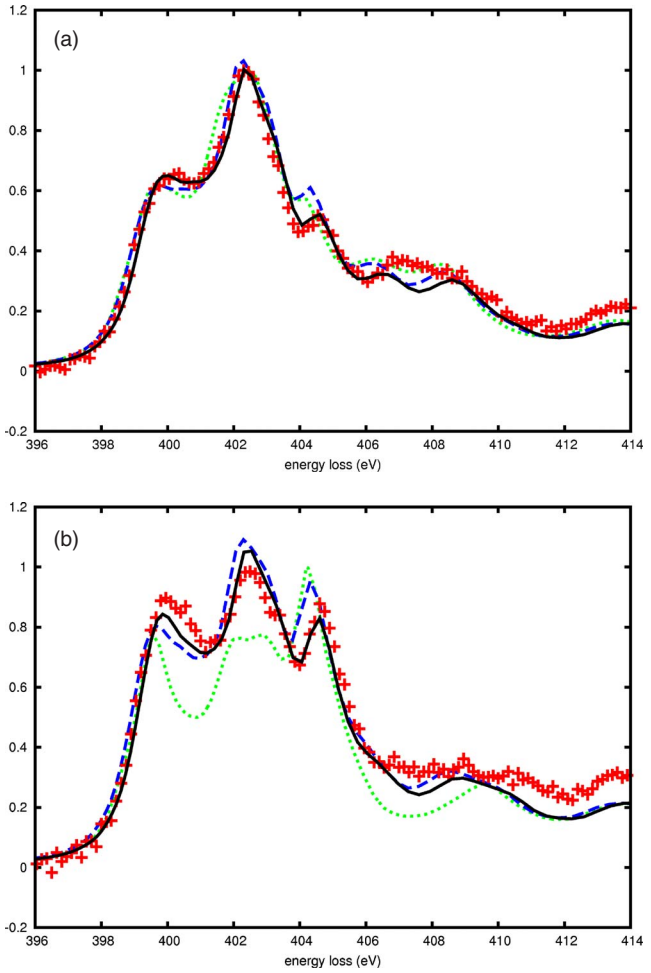

FIG. 3. (Color online) (a) N K-edge ELNES of GaN at 300-keV beam energy and collection angle 0.3 mrad and convergence angle 0.2 mrad, measured in [100] orientation. We compare the experiment [red+symbols; Moreno *et al.* (Ref. 23)] to different FEFF calculations: real-space calculation (green, short dashes), reciprocal space calculation (black, solid line), and a hybrid where the potentials were calculated in real space but the FMS calculation was done in reciprocal space (blue, long dashes). Spectra are aligned by hand and normalized at the second (403 eV) peak; and (b) for the [100] orientation and the collection angle is 0.4 mrad.

scattering t matrices were calculated in real space and the FMS calculation was then carried out in reciprocal space. Figure 3(b) shows the same edge measured and calculated in 001 orientation and the agreement is still very good. Essentially the same conclusions apply. We believe that remaining discrepancies between experiment and calculation can partly be attributed to the lack of full potential corrections in the scattering potentials.

Figure 4 shows a comparison of our reciprocal-space FEFF9 calculations to the supercell approach, calculated using the WIEN2K and TELNES2 programs.[11,24] Although the agreement between the WIEN2K calculation and the experimental spectrum is good by common standards, the onset is not described correctly, and it is unclear how well the feature at 405 eV is reproduced. It is of particular interest to study the edge onset. It can be seen that as the supercell grows in size, intensity slowly transfers to the onset, bringing it closer to

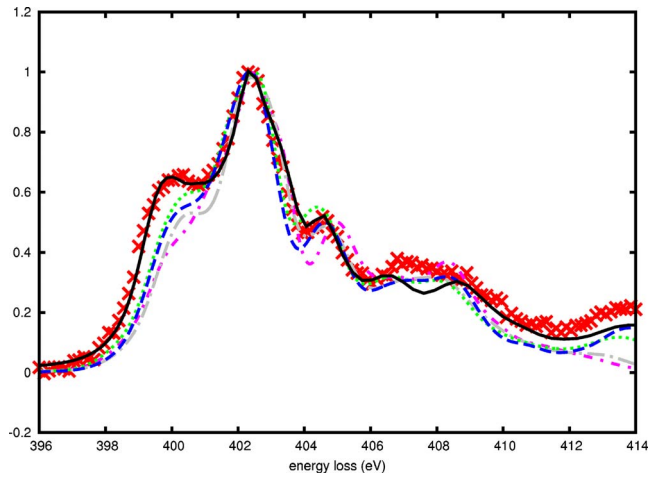

FIG. 4. (Color online) N K edge of GaN in the same experimental conditions as Fig. 3. The convergence of WIEN2K supercell size is studied and compared to experiment (red+symbols) and a FEFF9 calculation (black, solid line). WIEN2K spectra are shown for supercells of size $1\times1\times1$ (pink, short dash—dot), $2\times2\times1$ (gray, long dash—dot), $2\times2\times2$ (blue, long dashes), and $3\times3\times2$ (green, short dashes), in units of the regular unit cell. Spectra were aligned by hand and normalized to the second peak (403 eV).

the correct relative amplitude (if not energy) for the largest supercell we studied. The trend continues for even larger supercells ($4\times4\times3$); this is not included in the figure because basis set limitations made it difficult to calculate the spectrum reliably beyond the edge threshold. The FEFF9 calculation can be seen as the convergence point of a series of calculations of increasing supercell size.

Of course, one should not expect that the WIEN2K and FEFF9 calculations agree exactly with each other since the physics underlying each method is not identical. For example, FEFF9 uses a complex self-energy and spherical muffin-tin potentials while WIEN2K uses a real exchange-correlation potential and full nonspherical potentials. Finally, regarding computational efficiency, the FEFF9 spectrum was produced in about one CPU hour while the WIEN2K convergence study took several days on a computer cluster, with individual calculations ranging from about 1 h to 1 day with 5–12 CPU's.

While the reader may be interested in the relative speed of real and reciprocal space calculations, we are hesitant to make any sort of quantitative evaluation. For all of the examples shown in this paper, Eq. (14) presented a significant gain in efficiency over Eq. (13). However, these gains depends on the system, as systems with more complex unit cells will lead to slower **k**-space calculations, and real-space calculations scale with the inelastic mean-free path, which determines the cluster size needed for convergence. Similarly, it is very difficult to give general expectations for the time gains of reciprocal space FEFF compared to supercell calculations with band-structure codes, as there is no general guideline for how large a supercell needs to be. However, since the cost of a reciprocal space core hole FEFF calculation is little more than the cost of a ground-state calculation, we expect it to perform quite competitively.

VI. VALIDATION OF THE FINITE CLUSTER APPROXIMATION

The formal equivalence of the reciprocal space (long-range order) formalism and the real-space (short-range order) formalism has been established, e.g., by Schaich.[18] Formally, as the real-space calculations of electronic structure are taken to longer and longer range, they converge to the reciprocal space results. Since our approach in FEFF9 can calculate both real space and reciprocal space results (short and long range) within the same code, we can verify this equivalence directly using the same theoretical framework, approximations, and conventions for both ranges.

We present FEFF9 k-space XANES calculations of the Cu K edge in Fig. 5(a), thereby also illustrating the usefulness of our approach for XAS calculations. The agreement with experiment is excellent. This calculation can be compared directly to the real-space results presented elsewhere.[6] We show the convergence in reciprocal space as a function of the number of k vectors used for the BZ integration in Fig. 5(b), and in Fig. 5(c) the convergence in real space as a function of the number of atoms used for the finite-cluster FMS inversion. In Figs. 5(b) and 5(c) we have subtracted the smooth atomic background and show only the so-called fine structure, which is the quantity that requires convergence. One clearly sees that both calculations converge to the same result. Similar results were seen in the calculation of other ionization edges although typical k meshes are of the order $\sim10^3$ rather than $\sim10^2$.

The remaining question of efficiency of the RSGF approach for crystals thus depends on the "near sightedness" of matter.[25] The experience of the RSGF community shows that real-space calculations of the ground-state electronic structure of crystals typically converge quickly with cluster size, typically with about 50–100 atoms in the self-consistent calculations. In contrast, the convergence of the excited state electronic structure is set by the typical range of the mean-free path, which is typically between 5 and 20 Å in most materials. Thus an XAS or EELS spectrum is often fairly well converged for a cluster of about 150–300 atoms.[4,5,26] However, there is always the possibility of real-space finite cluster size artifacts in the calculation, which can be cumbersome to converge. For example, the diamond C K edge is very difficult to converge with respect to cluster size due to the much longer mean free paths for low Z atoms and shallow core holes. Such calculations can also become unreasonably inefficient, e.g., taking hours to calculate the density of states of diamond, which a band-structure code could do in minutes. While the focus of this paper is FSR calculation of EELS without the supercell, another important aim of our FEFF9 code is to avoid these inadequacies of the finite cluster real-space method for clusters.

VII. CONCLUSIONS

We have introduced a reciprocal-space extension to the real-space Green's function code FEFF9. This hybrid approach allows one to treat the ground state of a periodic system in reciprocal space and then add an appropriately screened-core hole in real space. This way we perform fast

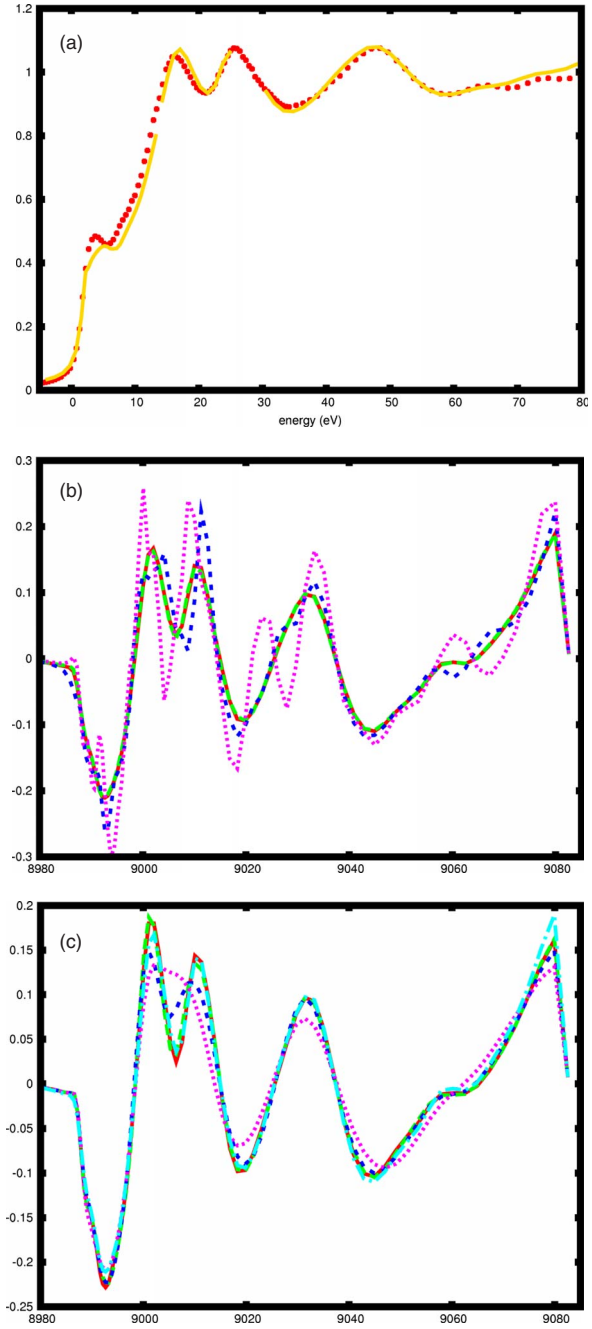

FIG. 5. (Color online) (a) K-space FEFF9 calculation of the Cu K edge (golden, solid line) compared to experimental XANES data (red+symbols). The calculation used 400 k points to sample the full Brillouin zone. Several newer FEFF9 features were used, including the MANYPOLE self-energy. (b) Long-range calculations: convergence of the Cu K edge as a function of the number of k points used to sample the full brillouin zone: 50 (pink, short dashes), 100 (blue, medium dashes), 200 (green, long dashes), and 2000 (red, solid line). Convergence is essentially reached at 200 k points. The quantity shown is the fine structure, i.e., the spectrum minus the smooth atomic background. (c) Short-range calculations: similarly, convergence of the fine structure in terms of the number of atoms in a real-space calculation: 50 (pink, short dashes), 100 (blue, medium dashes), 200 (green, long dashes), and 400 (red, solid line). Convergence is nearly reached at 400 atoms. This plot also shows the converged k-space result for comparison (cyan, long dash—dot).

calculations of ELNES and XANES for deep-core spectra without either making a finite cluster approximation or using a supercell. This sidesteps both supercell artifacts and supercell size convergence issues entirely. We have verified the validity of this approach by presenting excellent results for the N K edge of GaN and showing how they can be seen as the convergence point of DFT band-structure calculations of increasing supercell size. Additionally, we have demonstrated the equivalence of short-range and long-range methods by comparing real-space to reciprocal-space calculations of the Cu K edge using FEFF9 and showed that they converge to the same theoretical spectrum.

ACKNOWLEDGMENTS

This work was supported in part by the DOE under Grant No. DE-FG03–97ER45623 (J.J.R.) and was facilitated by the DOE Computational Materials Science Network. K. Jorissen gratefully acknowledges financial support by the F.W.O.-Vlaanderen as Research Assistant of the Research Foundation—Flanders. We wish to thank Z. Levine, E. Shirley, G. Hug., M. Jaouen, C. Hebert, M. S. Moreno, D. Lamoen, and P. Schattschneider for comments and suggestions, and particularly H. Ebert for his help and insights.

APPENDIX: CALCULATION OF THE KKR STRUCTURE FACTORS

The most efficient scheme for the calculation of the KKR structure factors defined in Eq. (3) is the Ewald summation technique.[27] It is also described in recent and more accessible papers.[28,29] However, these sources are limited to monatomic lattices. We here present the KKR structure factors of so-called complex crystals containing an arbitrary number of atoms in the unit cell.

We recall the definition of the structure factor

$$K_{\alpha\beta}(\boldsymbol{k}) \coloneqq G^0_{\alpha\beta}(\boldsymbol{k}) \coloneqq \lim_{N\to\infty} \frac{1}{N} \sum_{\substack{i=1 \\ i\neq j}}^{N} \sum_{\text{lattice vectors}} e^{i\boldsymbol{k}\cdot\boldsymbol{r}_{ij}} G^0_{i\alpha,j\beta}, \tag{A1}$$

where G^0 is the free propagator

$$G^0_{i\alpha,j\beta} = G^0[(\boldsymbol{r_i}+\boldsymbol{a_\alpha})-(\boldsymbol{r_j}+\boldsymbol{a_\beta})]. \tag{A2}$$

And the inverse relationship is

$$\Omega_{\mathrm{BZ}}^{-1}\int_{\mathrm{BZ}} d\boldsymbol{k} K_{\alpha\beta}(\boldsymbol{k}) e^{-i\boldsymbol{k}\cdot\boldsymbol{r}_{ij}} = N^{-1}\Omega_{\mathrm{BZ}}^{-1}\sum_{l\neq p} G^0_{l\alpha,p\beta}\int_{\mathrm{BZ}} d\boldsymbol{k} e^{i\boldsymbol{k}\cdot(\boldsymbol{r}_{lp}-\boldsymbol{r}_{ij})} = G^0_{i\alpha,j\beta}. \tag{A3}$$

Brute force calculation of $K_{\alpha\beta}$ by use of Eq. (A1) is very inefficient and can lead to convergence problems. For our purposes, the structure factor also needs to be expressed in an angular momentum basis $L,L'(L=l,m)$. We define a dummy function

$$G_{\alpha\beta}(\boldsymbol{R}) = -(4\pi)^{-1}\sum_s{}' \frac{e^{ip|\boldsymbol{R}-\boldsymbol{r}_s-\boldsymbol{a}_{\alpha\beta}|}}{\boldsymbol{R}-\boldsymbol{r}_s-\boldsymbol{a}_{\alpha\beta}} e^{i\boldsymbol{k}.\boldsymbol{r}_s}, \tag{A4}$$

where the prime on the summation symbol means that the sum runs over all lattice vectors excluding the term $\boldsymbol{r}_s=0$. The Fourier transform of $G_{\alpha\beta}$ is

$$\int_{\mathrm{BZ}} G_{\alpha\beta}(\boldsymbol{R}) e^{-i\boldsymbol{k}.\boldsymbol{r}_s} d\boldsymbol{k} = G^0[\boldsymbol{R}-(\boldsymbol{r}_s+\boldsymbol{a}_{\alpha\beta})] \quad \text{if} \quad \boldsymbol{r}_s \in \text{lattice};$$
$$= 0 \quad \text{otherwise}, \tag{A5}$$

where G^0 is the real-space free propagator (notice that this definition is not the Rehr-Albers normalization). The dummy function satisfies

$$K_{\alpha\beta} = \lim_{R\to 0} G_{\alpha\beta}(\boldsymbol{R}). \tag{A6}$$

Hence, an expansion of the form

$$G_{\alpha\beta}(\boldsymbol{R}=\boldsymbol{r}-\boldsymbol{r}') = \sum_L \sum_{L'} [i^{l-l'} B_{\alpha L\beta L'} j_l(pr) j_{l'}(pr') + p\,\delta_{LL'} j_l(pr) n_l(pr')] Y_L(\boldsymbol{r}) Y_{L'}(\boldsymbol{r}') \tag{A7}$$

will give us $K_{\alpha L\beta L'}$. However, as the Green's function is a function of $\mathbf{R}$, it can also be expanded as

$$G_{\alpha\beta}(\boldsymbol{R}) = -(4\pi)^{-1}\frac{\cos(pR)}{R} + \sum_L i^l D_{\alpha\beta L} j_l(pR) Y_L(\boldsymbol{R}), \tag{A8}$$

which is much simpler. The B coefficients can be recovered as

$$B_{\alpha L\beta L'} = 4\pi \sum_\Lambda D_{\alpha\beta\Lambda} C^\Lambda_{LL'}, \tag{A9}$$

where C are Wigner $3j$ symbols. The divergent terms in Eqs. (A7) and (A8) are only needed for $\mathbf{r}$ and $\mathbf{r}'$ in the same cell. FEFF9 has overlapping muffin-tin spheres so this is important even for $\mathbf{R}=0$. Finally, the spherical harmonics in Eqs. (A7) and (A8) are real.

Through the usual Ewald technique manipulations, the dummy function is written as

$$G_{\alpha\beta}(\boldsymbol{R}) = -(2\pi^{3/2})^{-1}\left[\sum_s{}' e^{i\boldsymbol{k}.\boldsymbol{r}_s}\left(\int_{\sqrt{\eta}/2}^{+\infty} e^{-(\boldsymbol{R}-\boldsymbol{r}_s-\boldsymbol{a}_{\alpha\beta})^2\xi^2+p^2/4\xi^2} d\xi\right) - \tau^{-1}\sum_n e^{i(\boldsymbol{K}_n+\boldsymbol{k}).(\boldsymbol{R}-\boldsymbol{a}_{\alpha\beta})}\frac{e^{-(\boldsymbol{K}_n+\boldsymbol{k})^2-p^2/\eta}}{(\boldsymbol{K}_n+\boldsymbol{k})^2-p^2} - \int_0^{\sqrt{\eta}/2} e^{-R^2\xi^2+p^2/4\xi^2} d\xi\right]. \tag{A10}$$

Then, projecting onto spherical harmonics and taking the limit $R\to 0$ (as $D_{\alpha\beta\,\mathrm{lm}}$ ought to be independent of R) gives the coefficients of Eq. (A8)

$$D_{\alpha\beta lm} = -4\pi\tau^{-1}\sum_n \frac{e^{-(k_n^2-p^2)/\eta}}{(k_n^2-p^2)} e^{-i\boldsymbol{k}_n.\boldsymbol{a}_{\alpha\beta}}\left(\frac{k_n}{p}\right)^l Y^*_{lm}(\boldsymbol{k}_n) + (\pi)^{-1}\delta_{l0}\delta_{m0}\int_0^{\sqrt{\eta}/2} e^{p^2/4\xi^2} d\xi - 2\pi^{-1/2}\sum_s{}' e^{i\boldsymbol{k}.\boldsymbol{r}_s} Y^*_{lm}[-i(\boldsymbol{r}_s+\boldsymbol{a}_{\alpha\beta})]$$
$$\times\left(\frac{-2i|\boldsymbol{r}_s+\boldsymbol{a}_{\alpha\beta}|}{p}\right)^l \int_{\sqrt{\eta}/2}^{+\infty} d\xi e^{-(\boldsymbol{r}_s+\boldsymbol{a}_{\alpha\beta})^2\xi+p^2/4\xi^2}\xi^{2l}. \tag{A11}$$

Equation (A11) is the main result of this appendix. It can be split in three parts

$$D_{\alpha\beta lm} = D^{(1)}_{lm} + D^{(3)}_{lm} + D^{(2)}_{lm}, \tag{A12}$$

where Greek indices were suppressed on the right-hand side. The latter two can be reworked into a more numerically convenient form.

$$D^{(3)}_{lm} = \delta_{l0}\delta_{m0}\frac{-1}{2\pi}\sqrt{\eta}\sum_{l=0}^{+\infty}\left(\frac{E}{\eta}\right)^l \frac{1}{l!(2l-1)}, \tag{A13}$$

$$D^{(2)}_{lm} = -2\pi^{-1/2}\sum_s{}' e^{i\boldsymbol{k}.\boldsymbol{r}_s} Y^*_{lm}[-i(\boldsymbol{r}_s+\boldsymbol{a}_{\alpha\beta})]\left(\frac{-2i|\boldsymbol{r}_s+\boldsymbol{a}_{\alpha\beta}|}{p}\right)^l \int_{\sqrt{\eta}/2}^{+\infty} d\xi e^{-(\boldsymbol{r}_s+\boldsymbol{a}_{\alpha\beta})^2\xi^2+p^2/4\xi^2}\xi^{2l}$$
$$= -\sqrt{\frac{\eta}{4\pi}}\sum_s{}' e^{i\boldsymbol{k}.\boldsymbol{r}_s} Y^*_{lm}[-i(\boldsymbol{r}_s+\boldsymbol{a}_{\alpha\beta})]\left(\frac{-i\eta|\boldsymbol{r}_s+\boldsymbol{a}_{\alpha\beta}|}{2p}\right)^l e^{-\eta/4|\boldsymbol{r}_s+\boldsymbol{a}_{\alpha\beta}|^2}\sum_n\left(\frac{p^2}{\eta}\right)^n \frac{1}{n!} f\left(l-n+\frac{1}{2}, \frac{\eta}{4}|\boldsymbol{r}_s+\boldsymbol{a}_{\alpha\beta}|^2\right). \tag{A14}$$

*Corresponding author; jjr@phys.washington.edu

[1] R. F. Egerton, *Electron Energy-Loss Spectroscopy in the Electron Microscope* (Plenum Press, New York, 1996).
[2] K. Jorissen, J. J. Rehr, and J. Verbeeck, Phys. Rev. B **81**, 155108 (2010).
[3] D. C. Koningsberger and R. Prins, *X-ray Absorption: Techniques of EXAFS, SEXAFS and XANES* (Plenum, New York, 1996).
[4] A. L. Ankudinov, B. Ravel, J. J. Rehr, and S. D. Conradson, Phys. Rev. B **58**, 7565 (1998).
[5] M. S. Moreno, K. Jorissen, and J. J. Rehr, Micron **38**, 1 (2007).
[6] J. J. Rehr, J. J. Kas, F. D. Vila, M. P. Prange, and K. Jorissen, Phys. Chem. Chem. Phys. **12**, 5503 (2010).
[7] J. J. Rehr, J. A. Soininen, and E. L. Shirley, Phys. Scr. **T115**, 207 (2005).
[8] G. Onida, L. Reining, and A. Rubio, Rev. Mod. Phys. **74**, 601 (2002).
[9] R. Del Sole, G. Adragna, V. Olevano, and L. Reining, Phys. Rev. B **67**, 045207 (2003).
[10] F. Sottile, F. Bruneval, A. G. Marinopoulos, L. K. Dash, S. Botti, V. Olevano, N. Vast, A. Rubio, and L. Reining, Int. J. Quantum Chem. **102**, 684 (2005).
[11] C. Hebert, Micron **38**, 12 (2007).
[12] L. V. Pourovskii, A. V. Ruban, L. Vitos, H. Ebert, B. Johansson, and I. A. Abrikosov, Phys. Rev. B **71**, 094415 (2005).
[13] M. Taillefumier, D. Cabaret, A. M. Flank, and F. Mauri, Phys. Rev. B **66**, 195107 (2002).
[14] J. L. Beeby, Proc. R. Soc. London, Ser. A **302**, 113 (1967).
[15] J. L. Beeby, Proc. R. Soc. London, Ser. A **279**, 82 (1964).
[16] J. Korringa, Physica (Amsterdam) **13**, 392 (1947).
[17] W. Kohn and N. Rostoker, Phys. Rev. **94**, 1111 (1954).
[18] W. L. Schaich, Phys. Rev. B **8**, 4028 (1973).
[19] J. J. Rehr, A. L. Ankudiniv, B. Ravel, and K. Jorissen, 2009, http://leonardo. phys.washington.edu/feff/html/documentation.html
[20] P. E. Blöchl, O. Jepsen, and O. K. Andersen, Phys. Rev. B **49**, 16223 (1994).
[21] J. T. Titantah, K. Jorissen, and D. Lamoen, Phys. Rev. B **69**, 125406 (2004).
[22] P. L. Potapov, K. Jorissen, D. Schryvers, and D. Lamoen, Phys. Rev. B **70**, 045106 (2004).
[23] M. S. Moreno, S. Lazar, H. W. Zandbergen, and R. F. Egerton, Phys. Rev. B **73**, 073308 (2006).
[24] P. Blaha, K. Schwarz, G. K. H. Madsen, D. Kvasnicka, and J. Luitz, *WIEN2K, An Augmented Plane Wave Plus Local Orbitals Program for Calculating Crystal Properties*, edited by K. Schwarz (Tech. Universitat Wien, Austria, 2001).
[25] E. Prodan and W. Kohn, Proc. Natl. Acad. Sci. U.S.A. **102**, 11635 (2005).
[26] B. Ravel and J. J. Rehr, J. Phys. IV **7**, C2–229 (1997).
[27] P. Ewald, Ann. Phys. **369**, 253 (1921).
[28] J. S. Faulkner, H. L. Davis, and H. W. Joy, Phys. Rev. **161**, 656 (1967).
[29] F. S. Ham and B. Segall, Phys. Rev. **124**, 1786 (1961).